



## Abstract

We used the MALTE-BOX model including near-explicit air chemistry and detailed aerosol dynamics to study the mechanisms of observed new particle formation events in the Jülich Plant Atmosphere Chamber. The modelled and measured H<sub>2</sub>SO<sub>4</sub> (sulphuric acid) concentrations agreed within a factor of two. The modelled total monoterpene concentration was in line with PTR-MS observations, and we provided the distributions of individual isomers of terpenes, when no measurements were available. The aerosol dynamic results supported the hypothesis that H<sub>2</sub>SO<sub>4</sub> is one of the critical compounds in the nucleation process. However, compared to kinetic H<sub>2</sub>SO<sub>4</sub> nucleation, nucleation involving OH oxidation products of monoterpenes showed a better agreement with the measurements, with  $R^2$  up to 0.97 between modelled and measured total particle number concentrations. The nucleation coefficient for kinetic H<sub>2</sub>SO<sub>4</sub> nucleation was  $2.1 \times 10^{-11} \text{ cm}^3 \text{ s}^{-1}$ , while the organic nucleation coefficient was  $9.0 \times 10^{-14} \text{ cm}^3 \text{ s}^{-1}$ . We classified the VOC oxidation products into two sub-groups including extremely low-volatility organic compounds (ELVOCs) and semi-volatile organic compounds (SVOCs). These ELVOCs and SVOCs contributed approximately equally to the particle volume production, whereas only ELVOCs made the smallest particles to grow in size. The model simulations revealed that the chamber walls constitute a major net sink of SVOCs on the first experiment day. However, the net wall SVOC uptake was gradually reduced because of SVOC desorption during the following days. Thus, in order to capture the observed temporal evolution of the particle number size distribution, the model needs to consider reversible gas-wall partitioning.

## 1 Introduction

New particle formation, including clustering of nanoparticles and their growth to larger sizes, has been observed world-widely in continental boundary layers and free troposphere (Kulmala et al., 2004; Mirme et al., 2010). Field observations, laboratory exper-

### Modelling the contribution of biogenic VOCs to new particle formation

L. Liao et al.

Title Page

Abstract

Introduction

Conclusions

References

Tables

Figures

◀

▶

◀

▶

Back

Close

Full Screen / Esc

Printer-friendly Version

Interactive Discussion



**Modelling the contribution of biogenic VOCs to new particle formation**

L. Liao et al.

Title Page

Abstract

Introduction

Conclusions

References

Tables

Figures

◀

▶

◀

▶

Back

Close

Full Screen / Esc

Printer-friendly Version

Interactive Discussion

iments and model simulations indicate that gaseous  $\text{H}_2\text{SO}_4$  plays an important role in atmospheric new particle formation, yet  $\text{H}_2\text{SO}_4$  alone appears not to be able to explain all the observed features of this process (Kulmala et al., 2000; Boy et al., 2003; Sipilä et al., 2010; Riipinen et al., 2007; Sihto et al., 2006; Kerminen et al., 2010; Kulmala et al., 2013, 2014). Basic compounds like ammonia and certain amines have been proposed to act as stabilizing compounds during clustering of nanoparticles (Berndt et al., 2010; Almeida et al., 2013; Kurtén et al., 2008), while subsequent steps of atmospheric new particle formation seem to rely on the presence of low-volatile organic compounds (e.g., Metzger et al., 2010; Paasonen et al., 2010; Riipinen et al., 2012; Ehn et al., 2014; Schobesberger et al., 2013).

Oxidation products of biogenic volatile organic compounds (BVOCs) constitute the largest source of secondary organic aerosol (SOA) in the global atmosphere (Tsigaridou and Kanakidou, 2003; Hallquist et al., 2009; Spracklen et al., 2011), accounting for the main composition of SOA condensational growth (VanReken et al., 2006; Hao et al., 2009; Riipinen et al., 2012). BVOC oxidation also produces extremely low volatile organic compounds essential to the new particle formation process (Ehn et al., 2014). The most abundant group of BVOCs, accounting for more than half of their global emissions, are terpenoids (Guenther et al., 1995). Terpenoids include compounds consisting of one to several isoprene units, e.g. isoprene ( $\text{C}_5\text{H}_8$ ), monoterpenes ( $\text{C}_{10}\text{H}_{16}$ ), and sesquiterpenes ( $\text{C}_{15}\text{H}_{24}$ ). Oxidation products of monoterpenes have shown substantial contribution to SOA formation (Hoffmann et al., 1997, 1998; Laaksonen et al., 2008), and low-volatile substances produced by sesquiterpene-ozone reactions may also initiate SOA formation (Bonn and Moortgat, 2003). Oxidation of isoprene leads to the formation of SOA (Surratt et al., 2006; Claeys et al., 2004), yet isoprene may also suppress the new particle formation process due to its high reactivity with OH (Kiehnler-Scharr et al., 2009). Overall, the exact contribution of BVOCs to SOA still remains uncertain, especially with respect to the initial steps of atmospheric new particle formation.



## Modelling the contribution of biogenic VOCs to new particle formation

L. Liao et al.

Title Page

Abstract

Introduction

Conclusions

References

Tables

Figures

◀

▶

◀

▶

Back

Close

Full Screen / Esc

Printer-friendly Version

Interactive Discussion

were placed in the JPAC plant chamber for more than one week before the initial experiment in order to allow them to adjust to the chamber environment. Tree emission was transferred into the reaction chamber, where  $O_3$  was added together with water vapor directly and OH was generated periodically by turning on the UV light. Discharge lamps (Osram HQI 400 W/D) were used for illumination to simulate the solar light spectrum in both chambers. Filters (OptoChem, type IR3) that reflect wavelengths between 750 and 1050 nm were used as heat shields to avoid infrared radiation inflicted plant overheating.

Ambient air was purified by an adsorption dryer (Zander, KEA 70) and a palladium catalyst (450 °C).  $O_3$ , NO,  $NO_2$  and VOC levels decreased significantly after passing the purification system. The flow through the plant chamber was  $115 \text{ L min}^{-1}$  from which  $20 \text{ L min}^{-1}$  were transferred to the reaction chamber. This flow was kept nearly constant by keeping the pressure drop constant. In addition, the  $10 \text{ L min}^{-1}$  flow containing ozone was added, controlled by a second flow controller.

Concentrations of  $O_3$ ,  $CO_2$  and  $H_2O$  were measured by commercial analytical instruments. Two Gas Chromatography Mass Spectrometer (GC-MS) systems were used, one to measure the VOC concentrations from  $C_5$  to  $C_{20}$  in the outflow air from the plant chamber (Heiden et al., 2003), and another to identify the OH concentration by determining the decrease in the concentration of a tracer compound in the reaction chamber (Kiendler-Scharr et al., 2009). Meanwhile, the VOC concentration was continuously measured by an on-line Proton Transfer Reaction Mass Spectrometer (PTR-MS) in the plant and reaction chamber. The gas phase  $H_2SO_4$  concentration in the reaction chamber was measured by a Chemical Ionization Mass Spectrometer (CIMS) (Petäjä et al., 2009; Mauldin et al., 1998). A prototype Airmodus Particle Size Magnifier (PSM) coupled with a TSI condensation particle counter (CPC) with a detection limit of ca. 1.6 nm was used to count the total number concentration of particles larger than 1.6 nm (Vanhanen et al., 2011). Also, another TSI CPC (TSI3022A) with a detection size limit of 7 nm was used to measure the total number concentration of particles larger than 7 nm.





mechanism from the original UHMA code, in which the particle formation rate ( $J$ ) is described as a power-law with the  $\text{H}_2\text{SO}_4$  concentration (Kulmala et al., 2006):

$$J = K \times [\text{H}_2\text{SO}_4]^2, \quad (1)$$

where  $K$  is termed as “kinetic nucleation coefficient”, including both the collision frequency and the probability of formation of a stable particle after the collision (Paasonen et al., 2010). In addition, based on the findings in Dal Maso et al. (2014), we updated the UHMA code to include the nucleation mechanism involving oxidation products of BVOCs, and we refer to it as organic nucleation in this study. As described by Dal Maso et al. (2014), data analysis showed that assuming both  $\text{H}_2\text{SO}_4$  and oxidation products of BVOCs are required for formation and activation of clusters produced corresponded best with observed results. Such a mechanism is described by the equation:

$$J = P \times [\text{H}_2\text{SO}_4] \times [\text{ELVOC}], \quad (2)$$

where  $P$  is the nucleation coefficient for organic nucleation (Paasonen et al., 2010). [ELVOC] refers to the concentration of ELVOC. In this study, we set the critical nucleation cluster size to be 1.5 nm in all the model runs (Kulmala et al., 2007; Zhang, 2010; Wang et al., 2013).

Schobesberger et al. (2013) found that both the  $\text{H}_2\text{SO}_4$  and oxidation products of monoterpenes were involved in the nucleation process. Ehn et al. (2014) suggested that ELVOC from the oxidation of  $\alpha$ -pinene participated in the initial steps of new particle formation. However, both studies were from well-controlled chamber experiments, with only a single BVOC compound investigated. Therefore, the identification of the ELVOC in the nucleation process remains uncertain, especially from mixtures of biogenic emissions. In this study, we did not try to identify any specific compounds involved in the nucleation, but rather aimed at finding differences in aerosol formation rates after the introduction of VOCs, as the compounds from MCM are too volatile to be in the range of ELVOC. Thus, we used representative compound  $\text{ELVOC}_{\text{OH}}$  (ELVOC from OH oxidations) as input of [ELVOC].

## Modelling the contribution of biogenic VOCs to new particle formation

L. Liao et al.

Title Page

Abstract

Introduction

Conclusions

References

Tables

Figures

◀

▶

◀

▶

Back

Close

Full Screen / Esc

Printer-friendly Version

Interactive Discussion



## Modelling the contribution of biogenic VOCs to new particle formation

L. Liao et al.

Title Page

Abstract

Introduction

Conclusions

References

Tables

Figures

◀

▶

◀

▶

Back

Close

Full Screen / Esc

Printer-friendly Version

Interactive Discussion



The information on e.g., saturation vapour pressures of condensable gas compounds is still insufficient and under investigation (Topping et al., 2007). Previous studies from the JPAC chamber experiments suggest that large amounts of ELVOCs is being formed from VOC oxidation, and that the reaction products contribute to the particle growth (Ehn et al., 2014). Here we used a simplified gas-particle partitioning model which classifies the terpene oxidation products into either ELVOCs or SVOCs. The reaction mechanisms can be described with following equations,



We then selected several compounds as the representatives of ELVOCs and SVOCs. Several criteria were used to select these compounds. First, compounds contained at least 9 carbon atoms, similar to the finding by Schobesberger et al. (2013). Second, selected compounds had the highest concentration among the VOC oxidation products, which should relatively represent the distribution of their reactants.

We selected two compounds from the first stable oxidation products of reactions between VOCs and OH where the full chemistry path was known, and then we defined these two compounds as the representatives of the  $\text{ELVOC}_{\text{OH}}$  and  $\text{SVOC}_{\text{OH}}$ . As a result,  $\text{ELVOC}_{\text{OH}}$  was APINAO2 (MCM name, oxidation product of  $\alpha$ -pinene by OH) and  $\text{SVOC}_{\text{OH}}$  was BPINAO2 (MCM name, OH oxidation product of  $\beta$ -pinene) in this study. The same approach was applied to the first stable oxidation products of reactions between VOCs and  $\text{O}_3$ . Pinonic acid was then selected as  $\text{ELVOC}_{\text{O}_3}$  and nopinone was chosen as  $\text{SVOC}_{\text{O}_3}$ . From the first stable oxidation products of reactions between VOCs and  $\text{NO}_3$ , we chose only NAPINAO2 (MCM name,  $\text{NO}_3$  oxidation product of  $\alpha$ -pinene) as  $\text{SVOC}_{\text{NO}_3}$ , and no ELVOC was taken into account.

To run the model, we set the saturation concentrations of  $\text{ELVOC}_{\text{OH}}$  and  $\text{ELVOC}_{\text{O}_3}$  to be three times larger than the  $\text{H}_2\text{SO}_4$  vapour ( $1 \text{ cm}^{-3}$ ), the same value as in Boy et al.

## Modelling the contribution of biogenic VOCs to new particle formation

L. Liao et al.

Title Page

Abstract

Introduction

Conclusions

References

Tables

Figures

◀

▶

◀

▶

Back

Close

Full Screen / Esc

Printer-friendly Version

Interactive Discussion

(2006), and the saturation concentrations of SVOCs to be  $5 \times 10^7 \text{ cm}^{-3}$ . In order to not systematically underestimate the total particle volume concentration, the formation of the five condensable compounds were multiplied with a fixed correction factor of two. We can then compare the modelled aerosol volume with the measurements, in a similar manner as Wang et al. (2013).

We used the fixed sectional approach to represent the particle size distribution in our simulation (Korhonen et al., 2004), which included 40 particle size bins.

### 2.2.3 Chamber wall loss

The original MALTE-BOX model includes two parameterizations for particle wall losses: one was from Crump and Seinfeld (1981) for mono-dispersed particles, and another was poly-dispersed particle theory by Park et al. (2001). We used the poly-dispersed particle loss mechanism in this study. The first order gas-wall deposition  $k_{g,w}$  ( $\text{s}^{-1}$ ) was also calculated from Park et al. (2001).

The reversible gas-wall partitioning of SVOCs was modelled by the following equation,

$$k_{w,g,i} = \frac{k_{g,w}}{(RT/\rho_{0,i}C_w)/(M_w\gamma_{w,i})}, \quad (4)$$

where  $k_{w,g}$  ( $\text{s}^{-1}$ ) is the desorption rate of SVOCs from the chamber surfaces out to the gas phase,  $C_w$  is an effective wall equivalent mass concentration of solvent which the organic compounds can dissolve into,  $M_w$  is the average molar mass of the solvent on the walls, and  $\gamma_{w,i}$  is the activity coefficient of compound  $i$  in the solvent. Compared with the values determined by Matsunaga and Ziemann (2010) for teflon chambers, we needed to use a ca. 3–4 order of magnitude smaller value ( $1 \times 10^{-8} \text{ mol m}^{-3}$ ) for the term  $C_w/(M_w\gamma_{w,i})$  in order to capture the observed reversible wall losses in the JPAC glass reaction chamber.

We assumed that ELVOCs should completely stick on the chamber surfaces, thus such reversible process was not considered for ELVOCs in this study.

## 2.2.4 Model input parameters

We executed the MALTE-BOX model for one measurement campaign conducted in the JPAC chamber. For analysing model results, we chose the first four continuous days from the whole measurement campaign because these days had continuous measurements, coverage of the dataset was complete, UV light-on period was the same, and chamber was stable.

The measured temperature and relative humidity (RH) in the JPAC reaction chamber were used directly in the model as input. As an example, values from the first four days are illustrated in Fig. 2. The temperature stabilized around noon on Day-1, after that the temperature was ca. 16 °C for all days. The RH had minor fluctuations during the experiment. RH was kept to ca. 60 % during UV-on periods for the first three days. On Day-4, the RH was around 55 %. In addition, 8 discharge lamps were used to simulate solar illumination on Day-1, but only 4 lamps were used on the remaining days.

Because ambient air in the JPAC chamber was purified by an adsorption dryer, the NO<sub>2</sub> concentration was set to 200 ppt<sub>v</sub>, and the NO concentration was set to 30 ppt<sub>v</sub> (Schimang et al., 2006). Other inorganic gases such as CO and SO<sub>2</sub> were not measured, thus some estimated constant values were used as input in the model. All the inorganic compound concentrations in the inflow used in the MALTE-BOX model are listed in Table 2. Concentrations of VOCs were based on the data from GC-MS and PTR-MS, and concentrations of VOC oxidation products were set to zero initially. As an example, concentrations of isoprene, monoterpenes and sesquiterpenes measured from the first four days are illustrated in Fig. 3. The monoterpene and sesquiterpene concentrations displayed a certain diurnal distribution pattern, because the discharge lamps mimicked sun light in the plant chamber. The total monoterpene concentration exceeded 4 ppb<sub>v</sub> on Day-1, and then decreased to a value below 2 ppb<sub>v</sub> on the following three days. In particular, the ocimene concentration was the highest on Day-1, which

can be explained by the fact that ocimene emission is light dependent (Owen et al., 2002), and the simulated solar light intensity from the discharge lamps was doubled on Day-1 in the plant chamber.

The isoprene concentration and the total sesquiterpene concentration were about an order of magnitude lower than the monoterpene concentration. Overall, the measured concentrations of terpenes were at similar levels as ambient air concentrations in boreal forest environments (Ruuskanen et al., 2009).

For particle data input, only the first measured particle size distribution from SMPS measurements was used for initialization of the model. In addition, the condensation sink calculated from SMPS measurements was used in the model to account for the condensation loss of sulphuric and nitric acid (Boy et al., 2006).

### 3 Results and discussion

#### 3.1 Gas-phase chemistry simulations

##### 3.1.1 O<sub>3</sub> and OH concentrations

In the JPAC reaction chamber, high OH concentrations were generated by periodically switching on the UV light. The UV light intensity in the JPAC reaction chamber was assumed stable and was set constant in our first model runs. The modelled O<sub>3</sub> concentration corresponded well with the measurements when the UV light was off (Fig. 4a). The modelled O<sub>3</sub> concentration reached steady state at the same level as the measurements, indicating that the dark reactions of VOCs were well represented in the model. Although the measured O<sub>3</sub> concentration showed a decrease at the beginning of Day-1, both modelled and measured O<sub>3</sub> concentrations reached levels of ca. 57 ppb<sub>v</sub> before the UV light was switched on. The O<sub>3</sub> concentration decreased sharply to about half of its initial value after the UV light was turned on, and then a continuous decrease in O<sub>3</sub> concentration was observed before the UV light was turned off.

**Modelling the contribution of biogenic VOCs to new particle formation**

L. Liao et al.

Title Page

Abstract

Introduction

Conclusions

References

Tables

Figures

◀

▶

◀

▶

Back

Close

Full Screen / Esc

Printer-friendly Version

Interactive Discussion

The modelled  $O_3$  reached a stable plateau after the sharp decrease (see the dash green line), whereas the measured  $O_3$  concentration continued to decrease until the UV light was switched off. As an explanation, the oxidation products from previous experiments may have been deposited and oligomerized on the lamp or chamber walls, and then photolyzed or thermally cracked introducing firstly a small time dependent extra sink for  $O_3$  in the chamber, and secondly a small increase in UV light intensity (this phenomenon disappeared after cleaning the UV lamp and did not reappear in succeeding campaigns, since the UV light lamp was placed inside a quartz tube with no direct contact to the reactants in the reaction chamber). To simulate this extra sink, we increased the UV intensity linearly in time so that the observed  $O_3$  was matched during phases with UV turned on. By applying 80 % UV light intensity increase, the modelled  $O_3$  concentrations (red dots in Fig. 4a) displayed the same distribution as the measured  $O_3$  concentration during UV-on periods. The measured  $O_3$  concentration decreased slightly more from Day-1 to Day-4. Nevertheless, we could reproduce the observations by applying the same 80 % UV light intensity increase for all four days.

The time series of modelled OH concentration is illustrated together with the estimated OH concentration by GC-MS in Fig. 4b. During UV-off periods, OH concentration was in the range  $10^5$ – $10^6$   $cm^{-3}$ , while after the UV light was turned on, OH concentration rapidly increased. The modelled OH concentration showed similar values as the estimated OH concentration after the first one-hour when the new steady state was well established. The transient of the OH concentration in the beginning cannot be detected by the marker measurements, because of limited time resolution of the GC-MS instrument. The second moderate increase in the OH concentration predicted by the model agreed better with the measurements, by applying 80 % UV light intensity increase during UV-on periods. In contrast, a decreasing trend in the OH concentration during UV-on periods was predicted by the model with constant UV light intensity. This justifies our previous assumption on increasing the UV light intensity. The experimentally determined OH concentration, after an hour when the UV light had been turned on, was  $5 \times 10^7$   $cm^{-3}$  on Day-1, about  $6 \times 10^7$   $cm^{-3}$  on Day-2, and about  $7$ – $8 \times 10^7$   $cm^{-3}$







previous studies, with the nucleation coefficient  $9.0 \times 10^{-14} \text{ cm}^3 \text{ s}^{-1}$ , similar to the value  $1.1 \times 10^{-13} \text{ cm}^3 \text{ s}^{-1}$  in Paasonen et al. (2010).

### 3.2.1 Sub-3 nm particle formation

The time series of the total number concentrations of particles larger than 1.6 nm ( $D_p > 1.6 \text{ nm}$ ) measured by PSM and modelled by both nucleation mechanisms are illustrated in Fig. 7. Two particle number concentration peaks were distinguished by the PSM measurements on the first three days when the UV light was turned on: one intensive particle burst followed by another moderate peak of formed particle numbers. Only a gradual increase in the particle number concentrations was found on Day-4. The particle number concentrations modelled by the kinetic  $\text{H}_2\text{SO}_4$  nucleation showed an opposite behaviour, increasing continuously during the UV-on periods on each day. The modelled total particle number concentrations from the organic nucleation mechanism showed similar distributions as the measurements on Day-1 and Day-4, with  $\pm 20\%$  difference. The model did not predict properly the first intensive peak of particle number concentrations on Day-2 and Day-3.

Figure 7 shows that the maximum of particle number concentrations modelled by the organic nucleation mechanism gradually decreased from Day-1 to Day-4, similar to the PSM measurements, whereas an opposite relation was seen from the average particle number concentrations modelled by the kinetic  $\text{H}_2\text{SO}_4$  nucleation. This agrees with the previous finding from Riccobono et al. (2014) that  $\text{H}_2\text{SO}_4$  and ELVOCs together play a major role in the new particle formation event. However, we did not see a better agreement between the modelled results and measurements when using the proposed nucleation mechanism ( $J = k_m[\text{H}_2\text{SO}_4]^2[\text{ELVOC}]$ ) by Riccobono et al. (2014). This is possibly due to the remaining difficulty of identifying which specific ELVOC compounds will contribute to the new particle formation.

The scatter plots of the total sub-3 nm particle number concentrations between model simulations and measurement are illustrated in Fig. 8, and the coefficients of

## Modelling the contribution of biogenic VOCs to new particle formation

L. Liao et al.

Title Page

Abstract

Introduction

Conclusions

References

Tables

Figures

◀

▶

◀

▶

Back

Close

Full Screen / Esc

Printer-friendly Version

Interactive Discussion

determination ( $R^2$ ) are listed in the figure legends. The smallest  $R^2$  value was 0.7 on Day-1 from the kinetic  $\text{H}_2\text{SO}_4$  nucleation and 0.77 on Day-3 from the organic nucleation. Overall, the determination coefficients from the organic nucleation showed relatively larger  $R^2$  than the coefficients from the kinetic  $\text{H}_2\text{SO}_4$  nucleation.

Although the modelled results could not fully represent the distributions of sub-3 nm particle number concentrations with any of the nucleation mechanisms, the simulations indicate that  $\text{H}_2\text{SO}_4$  and ELVOC<sub>OH</sub> were involved in the formation and growth of the homogeneously nucleated particles. Some other compounds, e.g. amines, may have also contributed to this process (Almeida et al., 2013; Kurtén et al., 2008), but the current model did not apply such chemistry, due to the lack of the amine measurements during this campaign.

### 3.2.2 SVOC gas phase-chamber wall partitioning and particle size distribution

In order to capture the condensational growth of formed particles, it is important to properly model the concentrations of gaseous precursors. By coupling the gas-wall-partitioning mechanism of SVOCs, we were able to model the total adsorption and desorption of SVOCs on the JPAC reaction chamber walls during the whole period. The total amounts of SVOCs adsorbed on the chamber walls, including SVOC<sub>OH</sub> and SVOC<sub>O<sub>3</sub></sub>, are illustrated in Fig. 9. The SVOCs desorbed from the chamber walls are also depicted in the same figure together with the concentrations of the total VOC oxidation products by OH and O<sub>3</sub>. The SVOCs adsorbed on the chamber walls increased significantly during the whole period, and their concentrations reached over an order of magnitude higher on Day-4. The increase in the SVOC<sub>O<sub>3</sub></sub> concentration was stronger than in the SVOC<sub>OH</sub> concentration.

The desorption of SVOCs from the chamber walls became substantial after Day-1, and reached a similar level as the summation of the ELVOCs and SVOCs which had not been deposited on the chamber walls.

## Modelling the contribution of biogenic VOCs to new particle formation

L. Liao et al.

Title Page

Abstract

Introduction

Conclusions

References

Tables

Figures

◀

▶

◀

▶

Back

Close

Full Screen / Esc

Printer-friendly Version

Interactive Discussion



## Modelling the contribution of biogenic VOCs to new particle formation

L. Liao et al.

Title Page

Abstract

Introduction

Conclusions

References

Tables

Figures

◀

▶

◀

▶

Back

Close

Full Screen / Esc

Printer-friendly Version

Interactive Discussion

The resulting contour plots of the time evolution of modelled particle number size distributions are depicted together with SMPS measurements in Fig. 10 for the kinetic  $\text{H}_2\text{SO}_4$  nucleation, and in Fig. 11 for the organic nucleation. For comparison, we executed also the model without gas-wall-partitioning of SVOCs, and the corresponding results are illustrated in Figs. 10b and 11b. The modelled time evolution of the particle size distributions from both nucleation mechanisms showed similar distributions as the measurements during the UV-on periods. However, the modelled particle size distributions from the organic nucleation mechanism showed better agreement with the measurements during the UV-off periods, as the particle number concentration was strongly over predicted by the kinetic  $\text{H}_2\text{SO}_4$  nucleation mechanism. Comparing with the modelled particle number size distributions without tracking the SVOC gas-wall-partitioning, it is conclusive that a substantial amount of SVOCs adsorbed on the JPAC reaction chamber walls during the measurement campaign, and the desorption of SVOCs from the walls significantly contributed to the growth of the freshly formed particles. This finding is in line with the results from Roldin et al. (2014); Zhang et al. (2014); Kokkola et al. (2014) in that the SVOC losses on chamber wall were reversible. Nevertheless, the model assumptions and the quantitative extent of the wall effects still need experimental verification e.g. by wall adsorption/desorption studies in JPAC. In any case it is clearly important to include such adsorption/desorption mechanism to properly describe the actual SOA formation from chamber measurements.

### 3.2.3 Particle volume production and compositions

We calculated the total particle volume concentrations from the SMPS measurements and modelled particle size distributions by assuming particles are spherical. The resulting time series of the particle volume concentration is illustrated in Fig. 12. Also, the scatter plots of the total particle volume concentrations between the modelled results from both nucleation mechanisms and the measurements are depicted in Fig. 13 for a closer look. Although the model underestimated the total particle volume concentration on Day-2, we were able to reproduce the aerosol volume production similar to the

measurements using both nucleation mechanisms overall, by considering a reversible SVOC gas-wall partitioning.

To investigate the average composition of particles during the different days, we took the total volume composition of particle volumes from average size distribution during the UV-on periods, and summed the compositions into three groups including H<sub>2</sub>SO<sub>4</sub>, ELVOCs, and SVOCs. The corresponding volume fractions of those three groups are depicted in Fig. 14. The *x* axis includes the first 30 particle size bins from the modelled particle size distribution, equalling particle size ranges from 1.5–250 nm in each sub-figure. H<sub>2</sub>SO<sub>4</sub> accounted for 100 % in the first particle size bin in all sub-figures. This was due to the technical solution of the MALTE-BOX model, as the initial activation clusters have been set as H<sub>2</sub>SO<sub>4</sub>. However, the volume fraction of H<sub>2</sub>SO<sub>4</sub> became totally negligible beside the first particle size bin, because the H<sub>2</sub>SO<sub>4</sub> concentration was several orders of magnitude lower than the ELVOC concentrations during the simulations, and we set the vapour pressure of H<sub>2</sub>SO<sub>4</sub> and ELVOCs to a similar level.

The topmost two panels show that ELVOCs dominated the total volume composition for small particles, while contributing around half of the particle volume compositions at larger particle sizes on Day-1 from both nucleation mechanisms, similar to the previous finding by Ehn et al. (2014). However, the average volume fraction of SVOCs to the total particle volumes changed from Day-1 to Day-4, with increasing amount of SVOCs desorbing from the chamber walls.

## 4 Summary and conclusion

In this study, we used the MALTE-BOX model to extend the earlier investigation on the formation mechanisms of aerosol particles from one measurement campaign conducted in the Jülich Plant Atmosphere Chamber. For the first time, we modelled the chemical and physical processes integrating both gas and particle phase simulations from the JPAC chamber measurements.

### Modelling the contribution of biogenic VOCs to new particle formation

L. Liao et al.

Title Page

Abstract

Introduction

Conclusions

References

Tables

Figures

◀

▶

◀

▶

Back

Close

Full Screen / Esc

Printer-friendly Version

Interactive Discussion



## Modelling the contribution of biogenic VOCs to new particle formation

L. Liao et al.

Title Page

Abstract

Introduction

Conclusions

References

Tables

Figures

◀

▶

◀

▶

Back

Close

Full Screen / Esc

Printer-friendly Version

Interactive Discussion



The gas phase simulation results showed that the modelled and measured  $\text{H}_2\text{SO}_4$  concentrations agreed within a factor of two. The modelled OH concentration was within the  $\pm 50\%$  uncertainty range of the estimated OH concentration from a tracer compound using GC-MS. The modelled  $\text{O}_3$  concentration was within 10–20% from the measurements. Monoterpene concentrations predicted from the model agreed well with the total monoterpene concentrations detected by PTR-MS. In addition, the model has shown that sesquiterpenes were strongly oxidized by  $\text{O}_3$  in the JPAC reaction chamber and minor oxidations by OH, even though the PTR-MS was not capable of providing such information on sesquiterpenes.

Our results suggest that  $\text{H}_2\text{SO}_4$  is one of the key compounds involved in the new particle formation, but cannot solely explain the new particle formation process. The nucleation coefficient predicted from the kinetic  $\text{H}_2\text{SO}_4$  nucleation was over an order of magnitude higher than in previous studies, while the organic nucleation coefficient better explained the experimental data, and its values were comparable with other studies.

We found that the SVOCs adsorbed on the chamber walls partly desorbed and substantially contributed to the SOA mass formation during Day-2 to Day-4 of the experiment. The modelled results, including particle growth and particle volume, strongly indicate that with every additional day of the model runs, all processes in the chamber were influenced by such chamber wall effects, which is in line with current discussions about wall effects in simulation chambers. As the SVOC contributes to SOA formation only at larger particle sizes, and the organic nucleation mechanisms depend on the ELVOC, results concerning new particle number formation are unaffected by the SVOC gas-wall-partitioning.

Overall, we have simulated the near-ambient atmospheric environment with the most up-to-date air chemistry and aerosol dynamics, the actual tree-emitted compounds were represented with model compounds, so our chemical reactions may not fully represent the actual chemistry in the JPAC reaction chamber. Our model was capable of predicting the average concentrations of both gas and particle phase components,



**Modelling the contribution of biogenic VOCs to new particle formation**

L. Liao et al.

Title Page

Abstract

Introduction

Conclusions

References

Tables

Figures

◀

▶

◀

▶

Back

Close

Full Screen / Esc

Printer-friendly Version

Interactive Discussion

Boy, M., Rannik, Ü., Lehtinen, K. E. J., Tarvainen, V., Hakola, H., and Kulmala, M.: Nucleation events in the continental boundary layer: long-term statistical analyses of aerosol relevant characteristics, *J. Geophys. Res.*, 108, 4667, doi:10.1029/2003JD003838, 2003. 27975

Boy, M., Hellmuth, O., Korhonen, H., Nilsson, E. D., ReVelle, D., Turnipseed, A., Arnold, F., and Kulmala, M.: MALTE – model to predict new aerosol formation in the lower troposphere, *Atmos. Chem. Phys.*, 6, 4499–4517, doi:10.5194/acp-6-4499-2006, 2006. 27976, 27978, 27981, 27984

Boy, M., Mogensen, D., Smolander, S., Zhou, L., Nieminen, T., Paasonen, P., Plass-Dülmer, C., Sipilä, M., Petäjä, T., Mauldin, L., Berresheim, H., and Kulmala, M.: Oxidation of SO<sub>2</sub> by stabilized Criegee intermediate (sCI) radicals as a crucial source for atmospheric sulfuric acid concentrations, *Atmos. Chem. Phys.*, 13, 3865–3879, doi:10.5194/acp-13-3865-2013, 2013. 27978, 27979, 27986

Claeys, M., Graham, B., Vas, G., Wang, W., Vermeylen, R., Pashynska, V., Cafmeyer, J., Guyon, P., Andreae, M. O., Artaxo, P., and Maenhaut, W.: Formation of secondary organic aerosols through photooxidation of isoprene, *Science*, 303, 1173–1176, 2004. 27975

Crump, J. G. and Seinfeld, J. H.: Turbulent deposition and gravitational sedimentation of an aerosol in a vessel of arbitrary shape, *J. Aerosol Sci.*, 12, 405–415, 1981. 27982

Dal Maso, M., Liao, L., Kiendler-Scharr, A., Kleist, E., Tillmann, R., Trimborn, A., Sipilä, M., Petäjä, T., Hakala, J., Lehtipalo, K., Junninen, H., Ehn, M., Vanhanen, J., Jyri, M., Wildt, J., Worsnop, D., Kulmala, M., and Mentel, T. F.: Direct observation of the influence of boreal BVOC and H<sub>2</sub>SO<sub>4</sub> on nanoparticle formation rates, submitted to *Atmos. Chem. Phys. Discuss.*, 2014. 27976, 27980

Damian, V., Sandu, A., Damian, M., Potra, F., and Carmichael, G. R.: The kinetic preprocessor KPP—a software environment for solving chemical kinetics, *Comput. Chem. Eng.*, 26, 1567–1579, 2002. 27978

Ehn, M., Thornton, J. A., Kleist, E., Sipilä, M., Junninen, H., Pullinen, I., Springer, M., Rubach, F., Tillmann, R., Lee, B., Lopez-Hilfiker, F., Andres, S., Acir, I.-H., Rissanen, M., Jokinen, T., Schobesberger, S., Kangasluoma, J., Kontkanen, J., Nieminen, T., Kurtén, T., Nielsen, L. B., Jorgensen, S., Kjaergaard, H. G., Canagaratna, M., Maso, M. D., Berndt, T., Petäjä, T., Wahner, A., Kerminen, V.-M., Kulmala, M., Worsnop, D. R., Wildt, J., and Mentel, T. F.: A large source of low-volatility secondary organic aerosol, *Nature*, 506, 476–479, 2014. 27975, 27980, 27981, 27992



**Modelling the contribution of biogenic VOCs to new particle formation**

L. Liao et al.

Title Page

Abstract

Introduction

Conclusions

References

Tables

Figures

◀

▶

◀

▶

Back

Close

Full Screen / Esc

Printer-friendly Version

Interactive Discussion

- Kerminen, V.-M., Petäjä, T., Manninen, H. E., Paasonen, P., Nieminen, T., Sipilä, M., Junninen, H., Ehn, M., Gagné, S., Laakso, L., Riipinen, I., Vehkamäki, H., Kurten, T., Ortega, I. K., Dal Maso, M., Brus, D., Hyvärinen, A., Lihavainen, H., Leppä, J., Lehtinen, K. E. J., Mirme, A., Mirme, S., Hörrak, U., Berndt, T., Stratmann, F., Birmili, W., Wiedensohler, A., Metzger, A., Dommen, J., Baltensperger, U., Kiendler-Scharr, A., Mentel, T. F., Wildt, J., Winkler, P. M., Wagner, P. E., Petzold, A., Minikin, A., Plass-Dülmer, C., Pöschl, U., Laaksonen, A., and Kulmala, M.: Atmospheric nucleation: highlights of the EUCAARI project and future directions, *Atmos. Chem. Phys.*, 10, 10829–10848, doi:10.5194/acp-10-10829-2010, 2010. 27975
- Kiendler-Scharr, A., Wildt, J., Dal Maso, M., Hohaus, T., Kleist, E., Mentel, T. F., Tillmann, R., Uerlings, R., Schurr, U., and Wahner, A.: New particle formation in forests inhibited by isoprene emissions, *Nature*, 461, 381–384, 2009. 27975, 27977
- Kokkola, H., Yli-Pirilä, P., Vesterinen, M., Korhonen, H., Keskinen, H., Romakkaniemi, S., Hao, L., Kortelainen, A., Joutsensaari, J., Worsnop, D. R., Virtanen, A., and Lehtinen, K. E. J.: The role of low volatile organics on secondary organic aerosol formation, *Atmos. Chem. Phys.*, 14, 1689–1700, doi:10.5194/acp-14-1689-2014, 2014. 27991
- Korhonen, H., Lehtinen, K. E. J., and Kulmala, M.: Multicomponent aerosol dynamics model UHMA: model development and validation, *Atmos. Chem. Phys.*, 4, 757–771, doi:10.5194/acp-4-757-2004, 2004. 27979, 27982
- Kulmala, M., Pirjola, U., and Makela, J. M.: Stable sulphate clusters as a source of new atmospheric particles, *Nature*, 404, 66–69, 2000. 27975
- Kulmala, M., Vehkamäki, H., Petäjä, T., Dal Maso, M., Lauri, A., Kerminen, V. M., Birmili, W., and McMurry, P. H.: Formation and growth rates of ultrafine atmospheric particles: a review of observations, *J. Aerosol Sci.*, 35, 143–176, 2004. 27974
- Kulmala, M., Lehtinen, K. E. J., and Laaksonen, A.: Cluster activation theory as an explanation of the linear dependence between formation rate of 3nm particles and sulphuric acid concentration, *Atmos. Chem. Phys.*, 6, 787–793, doi:10.5194/acp-6-787-2006, 2006. 27980
- Kulmala, M., Riipinen, I., Sipilä, M., Manninen, H. E., Petäjä, T., Junninen, H., Dal Maso, M., Mordas, G., Mirme, A., Vana, M., Hirsikko, A., Laakso, L., Harrison, R. M., Hanson, I., Leung, C., Lehtinen, K. E. J., and Kerminen, V. M.: Toward direct measurement of atmospheric nucleation, *Science*, 318, 89–92, 2007. 27980
- Kulmala, M., Nieminen, T., Chellapermal, R., Makkonen, R., Bäck, J., and Kerminen, V.-M.: Climate feedbacks linking the increasing atmospheric CO<sub>2</sub> concentration, BVOC emissions,

**Modelling the  
contribution of  
biogenic VOCs to  
new particle  
formation**

L. Liao et al.

Title Page

Abstract

Introduction

Conclusions

References

Tables

Figures

◀

▶

◀

▶

Back

Close

Full Screen / Esc

Printer-friendly Version

Interactive Discussion

aerosols and clouds in forest ecosystems, in: *Biology, Controls and Models of Tree Volatile Organic Compound Emissions*, Springer, Springer Netherlands, 489–508, 2013. 27975

Kulmala, M., Nieminen, T., Nikandrova, A., Lehtipalo, K., Manninen, H. E., Kajos, M. K., Kolar, P., Lauri, A., Petäjä, T., Krejci, R., Hansson, H.-C., Swietlicki, E., Lindroth, A., Christensen, T. R., Arneth, A., Hari, P., Bäck, J., Vesala, T., and Kerminen, V.-M.: CO<sub>2</sub>-induced terrestrial climate feedback mechanism: from carbon sink to aerosol source and back, *Bo-*  
real Environ. Res., 19, 122–131, 2014. 27975

Kurtén, T., Loukonen, V., Vehkamäki, H., and Kulmala, M.: Amines are likely to enhance neutral and ion-induced sulfuric acid-water nucleation in the atmosphere more effectively than ammonia, *Atmos. Chem. Phys.*, 8, 4095–4103, doi:10.5194/acp-8-4095-2008, 2008. 27975, 27990

Laaksonen, A., Kulmala, M., O'Dowd, C. D., Joutsensaari, J., Vaattovaara, P., Mikkonen, S., Lehtinen, K. E. J., Sogacheva, L., Dal Maso, M., Aalto, P., Petäjä, T., Sogachev, A., Yoon, Y. J., Lihavainen, H., Nilsson, D., Facchini, M. C., Cavalli, F., Fuzzi, S., Hoffmann, T., Arnold, F., Hanke, M., Sellegri, K., Umann, B., Junkermann, W., Coe, H., Allan, J. D., Alfarra, M. R., Worsnop, D. R., Riekkola, M. -L., Hyötyläinen, T., and Viisanen, Y.: The role of VOC oxidation products in continental new particle formation, *Atmos. Chem. Phys.*, 8, 2657–2665, doi:10.5194/acp-8-2657-2008, 2008. 27975

Matsunaga, A. and Ziemann, P. J.: Gas-wall partitioning of organic compounds in a Teflon film chamber and potential effects on reaction product and aerosol yield measurements, *Aerosol Sci. Tech.*, 44, 881–892, 2010. 27982

Mauldin, R., Frost, G., Chen, G., Tanner, D., Prevot, A., Davis, D., and Eisele, F.: OH measurements during the First Aerosol Characterization Experiment (ACE 1): observations and model comparisons, *J. Geophys. Res.*, 103, 16713–16729, doi:10.1029/98JD00882, 1998. 27977

Mentel, T. F., Wildt, J., Kiendler-Scharr, A., Kleist, E., Tillmann, R., Dal Maso, M., Fisseha, R., Hohaus, Th., Spahn, H., Uerlings, R., Wegener, R., Griffiths, P. T., Dinar, E., Rudich, Y., and Wahner, A.: Photochemical production of aerosols from real plant emissions, *Atmos. Chem. Phys.*, 9, 4387–4406, doi:10.5194/acp-9-4387-2009, 2009. 27976

Metzger, A., Verheggen, B., Dommen, J., Duplissy, J., Prevot, A. S., Weingartner, E., Riipinen, I., Kulmala, M., Spracklen, D. V., Carslaw, K. S., and Baltensperger U.: Evidence for the role of organics in aerosol particle formation under atmospheric conditions, *P. Natl. Acad. Sci. USA*, 107, 6646–6651, 2010. 27975

**Modelling the contribution of biogenic VOCs to new particle formation**

L. Liao et al.

[Title Page](#)[Abstract](#)[Introduction](#)[Conclusions](#)[References](#)[Tables](#)[Figures](#)[◀](#)[▶](#)[◀](#)[▶](#)[Back](#)[Close](#)[Full Screen / Esc](#)[Printer-friendly Version](#)[Interactive Discussion](#)

- Mirme, S., Mirme, A., Minikin, A., Petzold, A., Hörrak, U., Kerminen, V. -M., and Kulmala, M.: Atmospheric sub-3 nm particles at high altitudes, *Atmos. Chem. Phys.*, 10, 437–451, doi:10.5194/acp-10-437-2010, 2010. 27974
- Owen, S. M., Harley, P., Guenther, A., and Hewitt, C. N.: Light dependency of VOC emissions from selected Mediterranean plant species, *Atmos. Environ.*, 36, 3147–3159, 2002. 27984
- Paasonen, P., Nieminen, T., Asmi, E., Manninen, H. E., Petäjä, T., Plass-Dülmer, C., Flentje, H., Birmili, W., Wiedensohler, A., Hörrak, U., Metzger, A., Hamed, A., Laaksonen, A., Facchini, M. C., Kerminen, V.-M., and Kulmala, M.: On the roles of sulphuric acid and low-volatility organic vapours in the initial steps of atmospheric new particle formation, *Atmos. Chem. Phys.*, 10, 11223–11242, doi:10.5194/acp-10-11223-2010, 2010. 27975, 27980, 27988, 27989
- Park, S. H., Kim, H. O., Han, Y. T., Kwon, S. B., and Lee, K. W.: Wall loss rate of polydispersed aerosols, *Aerosol Sci. Tech.*, 35, 710–717, 2001. 27982
- Petäjä, T., Mauldin, III, R. L., Kosciuch, E., McGrath, J., Nieminen, T., Paasonen, P., Boy, M., Adamov, A., Kotiaho, T., and Kulmala, M.: Sulfuric acid and OH concentrations in a boreal forest site, *Atmos. Chem. Phys.*, 9, 7435–7448, doi:10.5194/acp-9-7435-2009, 2009. 27977, 27986
- Riccobono, F., Schobesberger, S., Scott, C. E., Dommen, J., Ortega, I. K., Rondo, L., Almeida, J. a., Amorim, A., Bianchi, F., Breitenlechner, M., David, A., Downard, A., Dunne, E. M., Duplissy, J., Ehrhart, S., Flagan, R. C., Franchin, A., Hansel, A., Junninen, H., Kajos, M., Keskinen, H., Kupc, A., Kürten, A., Kvashin, A. N., Laaksonen, A., Lehtipalo, K., Makhmutov, V., Mathot, S., Nieminen, T., Onnela, A., Petäjä, T., Praplan, A. P., Santos, F. D., Schallhart, S., Seinfeld, J. H., Sipilä, M., Spracklen, D. V., Stozhkov, Y., Stratmann, F., Tomé, A., Tsagkogeorgas, G., Vaattovaara, P., Viisanen, Y., Vrtala, A., Wagner, P. E., Weingartner, E., Wex, H., Wimmer, D., Carslaw, K. S., Curtius, J., Donahue, N. M., Kirkby, J., Kulmala, M., Worsnop, D. R., and Baltensperger, U.: Oxidation products of biogenic emissions contribute to nucleation of atmospheric particles, *Science*, 344, 717–721, 2014. 27989
- Riipinen, I., Sihto, S.-L., Kulmala, M., Arnold, F., Dal Maso, M., Birmili, W., Saarnio, K., Teinilä, K., Kerminen, V.-M., Laaksonen, A., and Lehtinen, K. E. J.: Connections between atmospheric sulphuric acid and new particle formation during QUEST III–IV campaigns in Heidelberg and Hyytiälä, *Atmos. Chem. Phys.*, 7, 1899–1914, doi:10.5194/acp-7-1899-2007, 2007. 27975, 27988

**Modelling the  
contribution of  
biogenic VOCs to  
new particle  
formation**

L. Liao et al.

Title Page

Abstract

Introduction

Conclusions

References

Tables

Figures

◀

▶

◀

▶

Back

Close

Full Screen / Esc

Printer-friendly Version

Interactive Discussion



- Riipinen, I., Yli-Juuti, T., Pierce, J. R., Petäjä, T., Worsnop, D. R., Kulmala, M., and Donahue, N. M.: The contribution of organics to atmospheric nanoparticle growth, *Nat. Geosci.*, 5, 453–458, 2012. 27975
- 5 Roldin, P., Eriksson, A. C., Nordin, E. Z., Hermansson, E., Mogensen, D., Rusanen, A., Boy, M., Swietlicki, E., Svenningsson, B., Zelenyuk, A., and Pagels, J.: Modelling non-equilibrium secondary organic aerosol formation and evaporation with the aerosol dynamics, gas- and particle-phase chemistry kinetic multilayer model ADCHAM, *Atmos. Chem. Phys.*, 14, 7953–7993, doi:10.5194/acp-14-7953-2014, 2014. 27991
- 10 Ruuskanen, T. M., Taipale, R., Rinne, J., Kajos, M. K., Hakola, H., and Kulmala, M.: Quantitative long-term measurements of VOC concentrations by PTR-MS: annual cycle at a boreal forest site, *Atmos. Chem. Phys. Discuss.*, 9, 81–134, doi:10.5194/acpd-9-81-2009, 2009. 27984
- Saunders, S. M., Jenkin, M. E., Derwent, R. G., and Pilling, M. J.: Protocol for the development of the Master Chemical Mechanism, MCM v3 (Part A): tropospheric degradation of non-aromatic volatile organic compounds, *Atmos. Chem. Phys.*, 3, 161–180, doi:10.5194/acp-3-161-2003, 2003. 27978
- 15 Schimang, R., Folkers, A., Kleffmann, J., Kleist, E., Miebach, M., and Wildt, J.: Uptake of gaseous nitrous acid (HONO) by several plant species, *Atmos. Environ.*, 40, 1324–1335, 2006. 27976, 27983
- Schobesberger, S., Junninen, H., Bianchi, F., Lönn, G., Ehn, M., Lehtipalo, K., Dommen, J., Ehrhart, S., Ortega, I. K., Franchin, A., Nieminen, T., Riccobono, F., Hutterli, M., Duplissy, J., Almeida, J., Amorim, A., Breitenlechner, M., Downard, A. J., Dunne, E. M., Flagan, R. C., Kajos, M., Keskinen, H., Kirkby, J., Kupc, A., Kürten, A., Kurtén, T., Laaksonen, A., Mathot, S., Onnela, A., Praplan, A. P., Rondo, L., Santos, F. D., Schallhart, S., Schnitzhofer, R., Sipilä, M., Tomé, A., Tsagkogeorgas, G., Vehkamäki, H., Wimmer, D., Baltensperger, U., Carslaw, K. S., Curtius, J., Hansel, A., Petäjä, T., Kulmala, M., Donahue, N. M., and Worsnop, D. R.: Molecular understanding of atmospheric particle formation from sulfuric acid and large oxidized organic molecules, *P. Natl. Acad. Sci. USA*, 110, 17223–17228, 2013. 27975, 27980, 27981
- 25 30 Sihto, S.-L., Kulmala, M., Kerminen, V.-M., Dal Maso, M., Petäjä, T., Riipinen, I., Korhonen, H., Arnold, F., Janson, R., Boy, M., Laaksonen, A., and Lehtinen, K. E. J.: Atmospheric sulphuric acid and aerosol formation: implications from atmospheric measurements for nucleation and early growth mechanisms, *Atmos. Chem. Phys.*, 6, 4079–4091, doi:10.5194/acp-6-4079-2006, 2006. 27975

**Modelling the contribution of biogenic VOCs to new particle formation**

L. Liao et al.

Title Page

Abstract

Introduction

Conclusions

References

Tables

Figures

◀

▶

◀

▶

Back

Close

Full Screen / Esc

Printer-friendly Version

Interactive Discussion

- Sipilä, M., Berndt, T., Petäjä, T., Brus, D., Vanhanen, J., Stratmann, F., Patokoski, J., Mauldin, Roy, L., I., Hyvarinen, A.-P., Lihavainen, H., and Kulmala, M.: The role of sulfuric acid in atmospheric nucleation, *Science*, 327, 1243–1246, 2010. 27975
- Spracklen, D. V., Jimenez, J. L., Carslaw, K. S., Worsnop, D. R., Evans, M. J., Mann, G. W., Zhang, Q., Canagaratna, M. R., Allan, J., Coe, H., McFiggans, G., Rap, A., and Forster, P.: Aerosol mass spectrometer constraint on the global secondary organic aerosol budget, *Atmos. Chem. Phys.*, 11, 12109–12136, doi:10.5194/acp-11-12109-2011, 2011. 27975
- Surratt, J. D., Murphy, S. M., Kroll, J. H., Ng, N. L., Hildebrandt, L., Sorooshian, A., Szmigielski, R., Vermeylen, R., Maenhaut, W., Claeys, M., Flagan, R. C., and Seinfeld, J. H.: Chemical composition of secondary organic aerosol formed from the photooxidation of isoprene, *J. Phys. Chem. A*, 110, 9665–9690, 2006. 27975
- Topping, D. O., McFiggans, G. B., Kiss, G., Varga, Z., Facchini, M. C., Decesari, S., and Mircea, M.: Surface tensions of multi-component mixed inorganic/organic aqueous systems of atmospheric significance: measurements, model predictions and importance for cloud activation predictions, *Atmos. Chem. Phys.*, 7, 2371–2398, doi:10.5194/acp-7-2371-2007, 2007. 27981
- Tsigaridis, K. and Kanakidou, M.: Global modelling of secondary organic aerosol in the troposphere: a sensitivity analysis, *Atmos. Chem. Phys.*, 3, 1849–1869, doi:10.5194/acp-3-1849-2003, 2003. 27975
- Vanhanen, J., Mikkilä, J., Lehtipalo, K., Sipilä, M., Manninen, H. E., Siivola, E., Petäjä, T., and Kulmala, M.: Particle size magnifier for nano-CN detection, *Aerosol Sci. Tech.*, 45, 533–542, 2011. 27977
- VanReken, T. M., Greenberg, J. P., Harley, P. C., Guenther, A. B., and Smith, J. N.: Direct measurement of particle formation and growth from the oxidation of biogenic emissions, *Atmos. Chem. Phys.*, 6, 4403–4413, doi:10.5194/acp-6-4403-2006, 2006. 27975
- Wang, Z. B., Hu, M., Mogensen, D., Yue, D. L., Zheng, J., Zhang, R. Y., Liu, Y., Yuan, B., Li, X., Shao, M., Zhou, L., Wu, Z. J., Wiedensohler, A., and Boy, M.: The simulations of sulfuric acid concentration and new particle formation in an urban atmosphere in China, *Atmos. Chem. Phys.*, 13, 11157–11167, doi:10.5194/acp-13-11157-2013, 2013. 27980, 27982
- Zhang, R.: Getting to the critical nucleus of aerosol formation, *Science*, 328, 1366–1367, 2010. 27980

Zhang, X., Cappa, C. D., Jathar, S. H., McVay, R. C., Ensberg, J. J., Kleeman, M. J., and Seinfeld, J. H.: Influence of vapor wall loss in laboratory chambers on yields of secondary organic aerosol, P. Natl. Acad. Sci. USA, 111, 5802–5807, 2014. 27991

ACPD

14, 27973–28018, 2014

**Modelling the contribution of biogenic VOCs to new particle formation**

L. Liao et al.

Title Page

Abstract

Introduction

Conclusions

References

Tables

Figures



Back

Close

Full Screen / Esc

Printer-friendly Version

Interactive Discussion



## Modelling the contribution of biogenic VOCs to new particle formation

L. Liao et al.

Title Page

Abstract

Introduction

Conclusions

References

Tables

Figures

◀

▶

◀

▶

Back

Close

Full Screen / Esc

Printer-friendly Version

Interactive Discussion

**Table 1.** The VOCs measured by GC-MS which were included as input in the MALTE-BOX model for the air chemistry module. The “other MTs” and “other SQTs” refer to other monoterpenes and sesquiterpenes than those specified in the table, respectively.

isoprene				
$\alpha$ -pinene	$\beta$ -pinene	myrcene	sabinene	camphene
ocimene	carene	$\alpha$ -terpinene	$\gamma$ -terpinene	$\alpha$ -phellandrene
$\beta$ -phellandrene	terpinolene	tricyclene	other MTs	
farnesene	$\beta$ -caryophyllene	$\alpha$ -longipinene	$\gamma$ -cadinene	other SQTs
2-butanol	hexanal	toluene	eucalyptol	nonanal
bornyl acetate	methyl salicylate			

## Modelling the contribution of biogenic VOCs to new particle formation

L. Liao et al.

Title Page

Abstract

Introduction

Conclusions

References

Tables

Figures

◀

▶

◀

▶

Back

Close

Full Screen / Esc

Printer-friendly Version

Interactive Discussion



**Table 2.** The constant concentration and flow rate of each inorganic gas compound as input in the MALTE-BOX model.

Compound	NO	NO <sub>2</sub>	NO <sub>3</sub>	SO <sub>2</sub>	O <sub>3</sub>	CO
Concentration (ppb <sub>v</sub> )	0.03	0.2	0.3	0.015	200	100
Flow rate (L min <sup>-1</sup> )	31	31	31	31	11	31

## Modelling the contribution of biogenic VOCs to new particle formation

L. Liao et al.

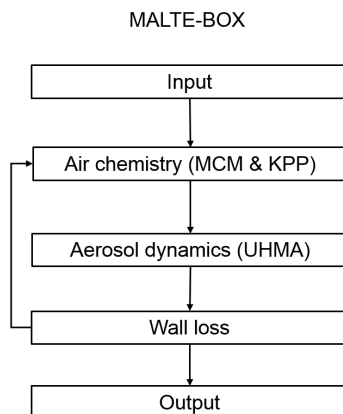


**Figure 1.** Schematic picture of the MALTE-BOX model structure.

Title Page

Abstract

Introduction

Conclusions

References

Tables

Figures

◀

▶

◀

▶

Back

Close

Full Screen / Esc

Printer-friendly Version

Interactive Discussion

## Modelling the contribution of biogenic VOCs to new particle formation

L. Liao et al.

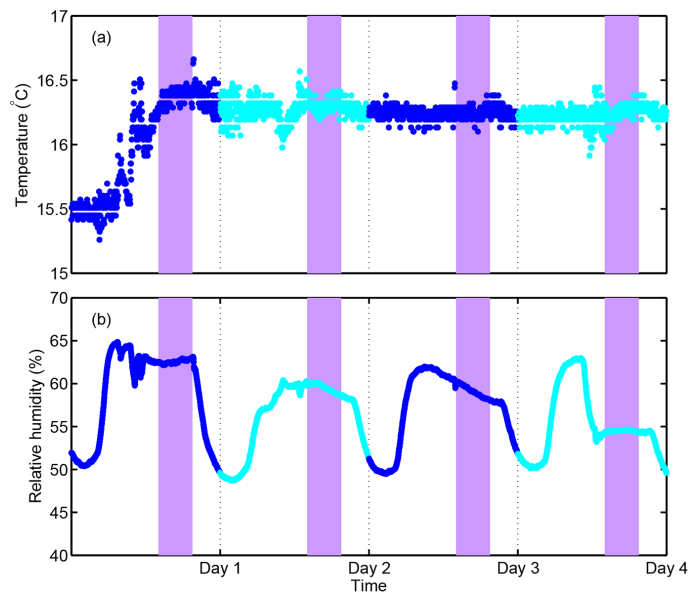


**Figure 2.** Temperature (a) and relative humidity (b) measured on the first four days in the JPAC reaction chamber. The purple bars indicate UV-on periods during the measurements.

Title Page

Abstract

Introduction

Conclusions

References

Tables

Figures

◀

▶

◀

▶

Back

Close

Full Screen / Esc

Printer-friendly Version

Interactive Discussion

## Modelling the contribution of biogenic VOCs to new particle formation

L. Liao et al.

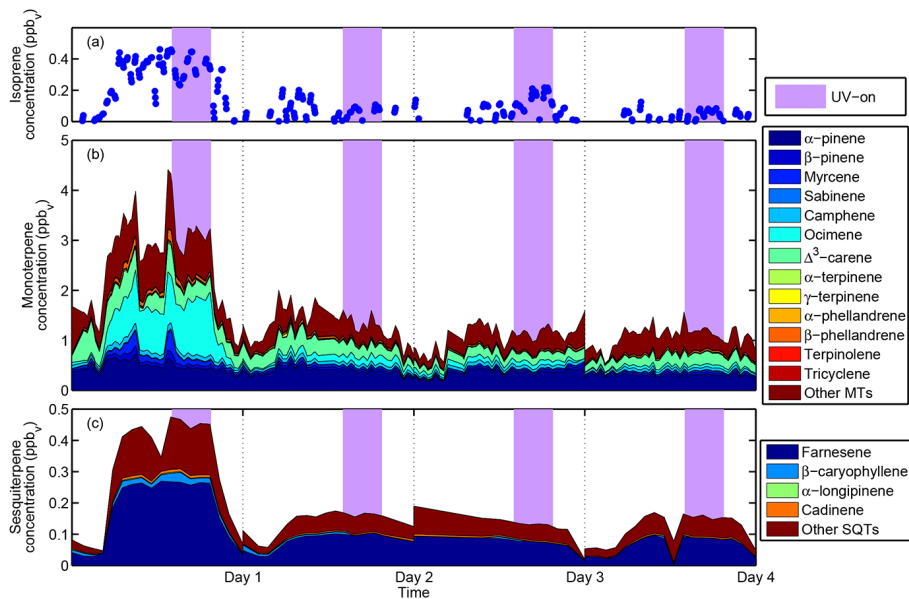


**Figure 3.** Isoprene (a), monoterpene (b), and sesquiterpene (c) concentrations measured from the outlet air of the JPAC plant chamber. The purple bars indicate UV-on periods during the measurements in all sub-figures.

Title Page

Abstract

Introduction

Conclusions

References

Tables

Figures

◀

▶

◀

▶

Back

Close

Full Screen / Esc

Printer-friendly Version

Interactive Discussion

## Modelling the contribution of biogenic VOCs to new particle formation

L. Liao et al.

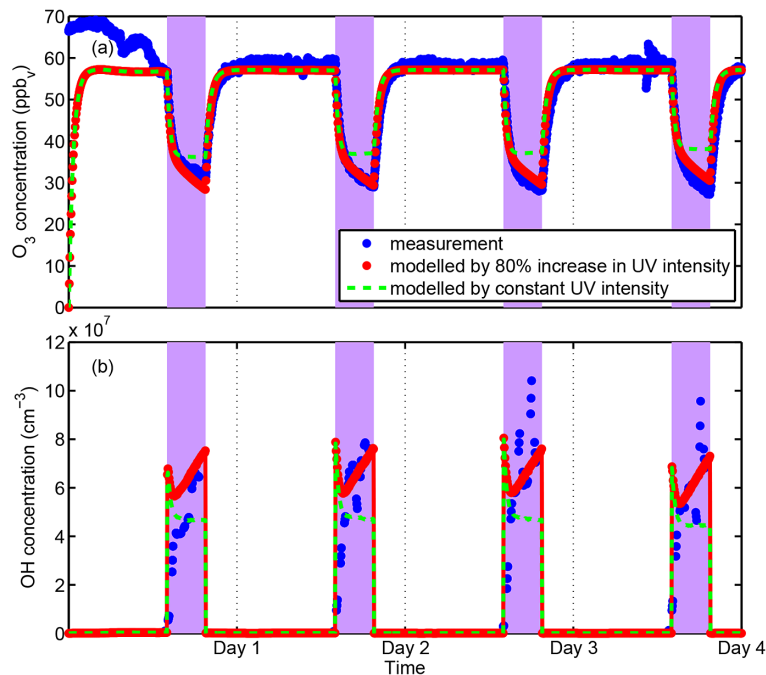


**Figure 4.** (a) O<sub>3</sub> concentrations modelled and measured in the JPAC reaction chamber. The green dash line indicates the modelled O<sub>3</sub> concentrations applying constant UV light intensity, and the red markers are the modelled O<sub>3</sub> concentrations applying 80 % UV light intensity increase during UV-on periods for all days. (b) OH radical concentrations modelled and estimated from tracer compound using GC-MS in the JPAC reaction chamber. The green dash line indicates the modelled OH concentrations applying constant UV intensity, and the red markers are the modelled OH concentrations applying 80 % UV intensity increase during UV-on periods. The purple bars indicate UV-on periods during the measurements in both sub-figures, and the blues markers illustrate data from measurements.

Title Page

Abstract

Introduction

Conclusions

References

Tables

Figures

◀

▶

◀

▶

Back

Close

Full Screen / Esc

Printer-friendly Version

Interactive Discussion

## Modelling the contribution of biogenic VOCs to new particle formation

L. Liao et al.

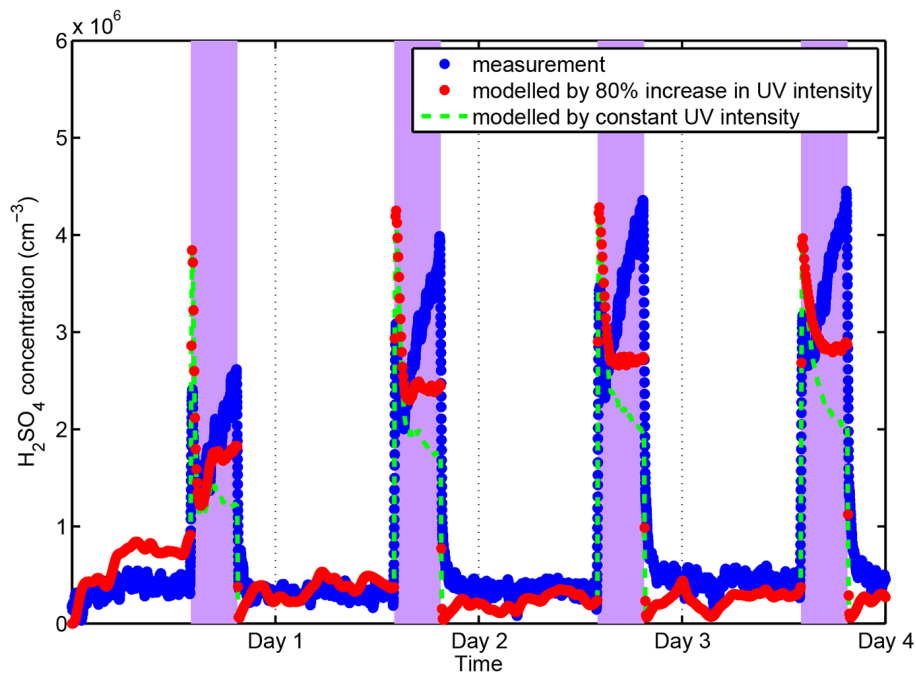


**Figure 5.**  $\text{H}_2\text{SO}_4$  concentrations modelled and measured in the JPAC reaction chamber. The green dash line indicates the modelled  $\text{H}_2\text{SO}_4$  concentrations applying constant UV intensity, and the red markers are the modelled  $\text{H}_2\text{SO}_4$  concentrations applying 80% UV intensity increase during UV-on periods for all days. The purple bars indicate UV-on periods during the measurements.

[Title Page](#)[Abstract](#)[Introduction](#)[Conclusions](#)[References](#)[Tables](#)[Figures](#)[◀](#)[▶](#)[◀](#)[▶](#)[Back](#)[Close](#)[Full Screen / Esc](#)[Printer-friendly Version](#)[Interactive Discussion](#)

## Modelling the contribution of biogenic VOCs to new particle formation

L. Liao et al.

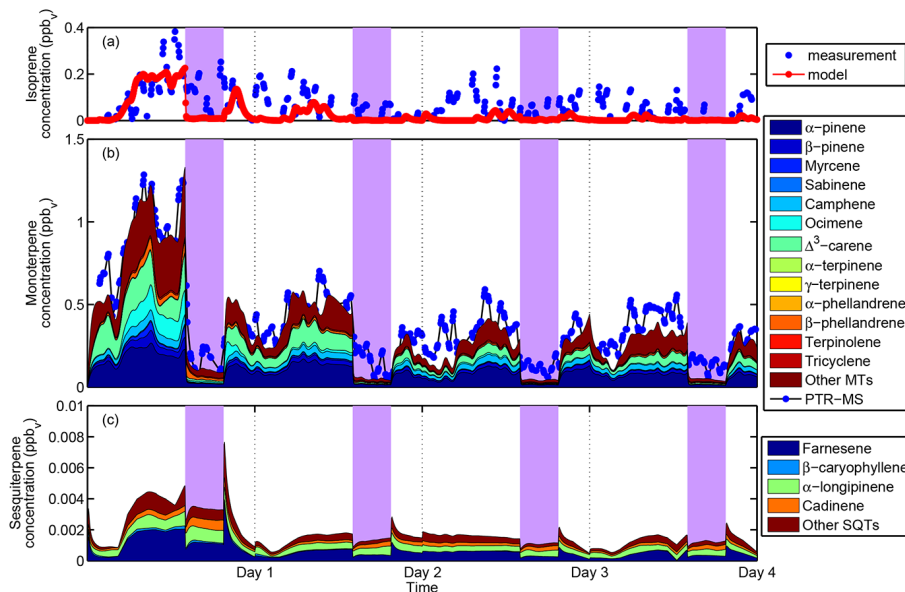


**Figure 6.** Isoprene (a), monoterpene (b), and sesquiterpene (c) concentrations modelled together with the isoprene and monoterpene concentrations measured by PTR-MS in the JPAC reaction chamber. The purple bars indicate UV-on periods during the measurements. The blue markers illustrate data from the measurements, and the red dots are the modelled isoprene concentrations in the topmost panel.

Title Page

Abstract

Introduction

Conclusions

References

Tables

Figures

◀

▶

◀

▶

Back

Close

Full Screen / Esc

Printer-friendly Version

Interactive Discussion

## Modelling the contribution of biogenic VOCs to new particle formation

L. Liao et al.

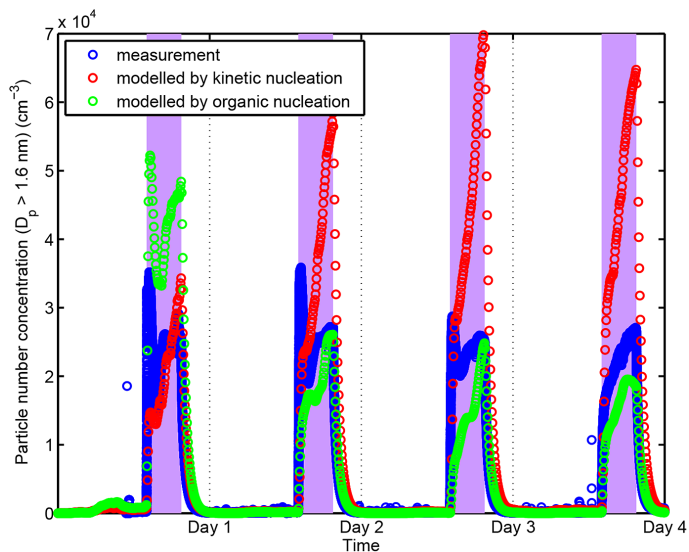


**Figure 7.** Time series of the total number concentrations of particles larger than 1.6 nm in diameter. The blue markers indicate particle number concentrations measured by PSM. The red markers represent particle number concentrations predicted by the kinetic  $\text{H}_2\text{SO}_4$  nucleation mechanism, and the green markers are particle number concentrations predicted by the organic nucleation mechanism. The purple bars indicate UV-on periods during the measurements.

[Title Page](#)[Abstract](#)[Introduction](#)[Conclusions](#)[References](#)[Tables](#)[Figures](#)[◀](#)[▶](#)[◀](#)[▶](#)[Back](#)[Close](#)[Full Screen / Esc](#)[Printer-friendly Version](#)[Interactive Discussion](#)

## Modelling the contribution of biogenic VOCs to new particle formation

L. Liao et al.

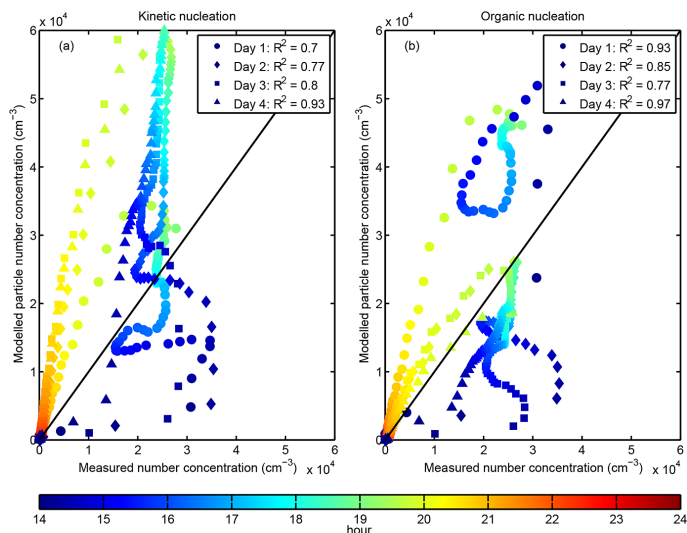


**Figure 8.** Modelled number concentrations of particles larger than 1.6 nm **(a)** using kinetic  $\text{H}_2\text{SO}_4$  nucleation and **(b)** using organic nucleation vs. total particle number concentrations measured by PSM. The black lines indicate the 1 : 1 ratio in both sub figures. The coefficients of determination ( $R^2$ ) are listed in the legends. The color bar indicates hours of the day.

## Modelling the contribution of biogenic VOCs to new particle formation

L. Liao et al.

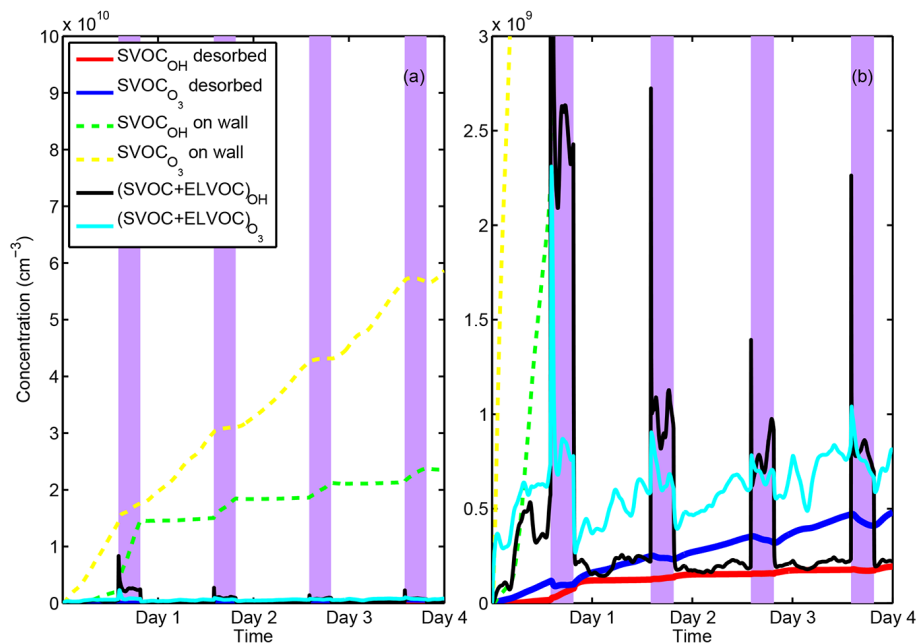


**Figure 9.** Time series of the total amount of SVOCs desorbed from the chamber wall, SVOCs on the chamber walls, and the total amount of VOC oxidation products by OH and O<sub>3</sub>. The right panel is the y axis zoom-in figure from the left panel.

## Modelling the contribution of biogenic VOCs to new particle formation

L. Liao et al.

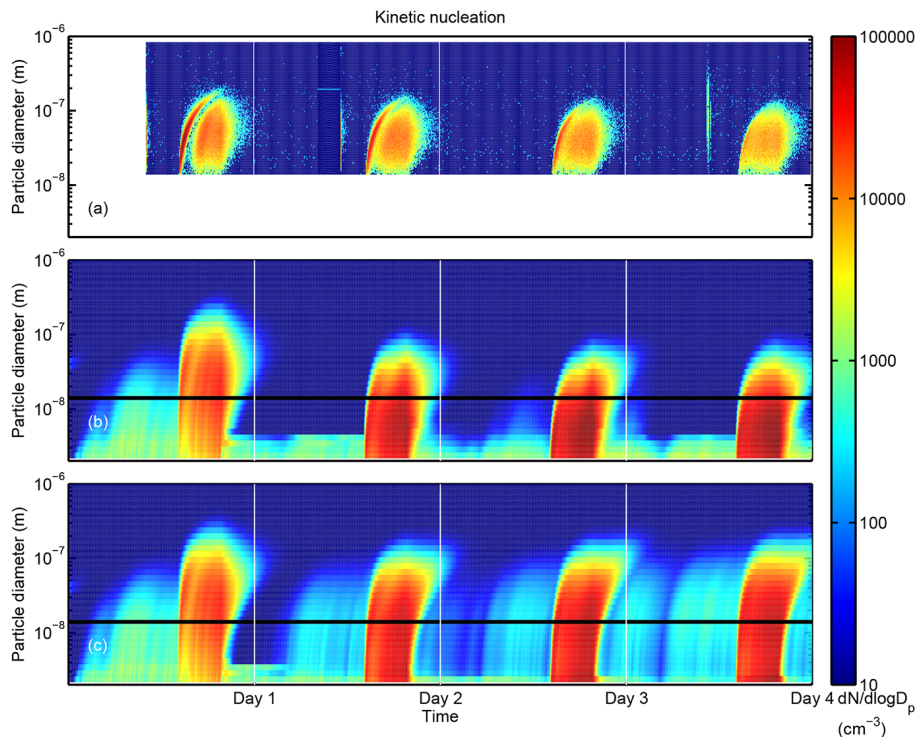


**Figure 10.** Contour plots of aerosol particle number size distributions as function of time from the SMPS measurements **(a)**, and contour plots of aerosol particle number size distributions as function of time from the MALTE-BOX model predicted using kinetic  $\text{H}_2\text{SO}_4$  nucleation without **(b)** and with **(c)** SVOC gas-wall-partitioning. The black lines indicate the smallest particle size measured by SMPS in all sub-figures.

Title Page

Abstract

Introduction

Conclusions

References

Tables

Figures

◀

▶

◀

▶

Back

Close

Full Screen / Esc

Printer-friendly Version

Interactive Discussion

## Modelling the contribution of biogenic VOCs to new particle formation

L. Liao et al.

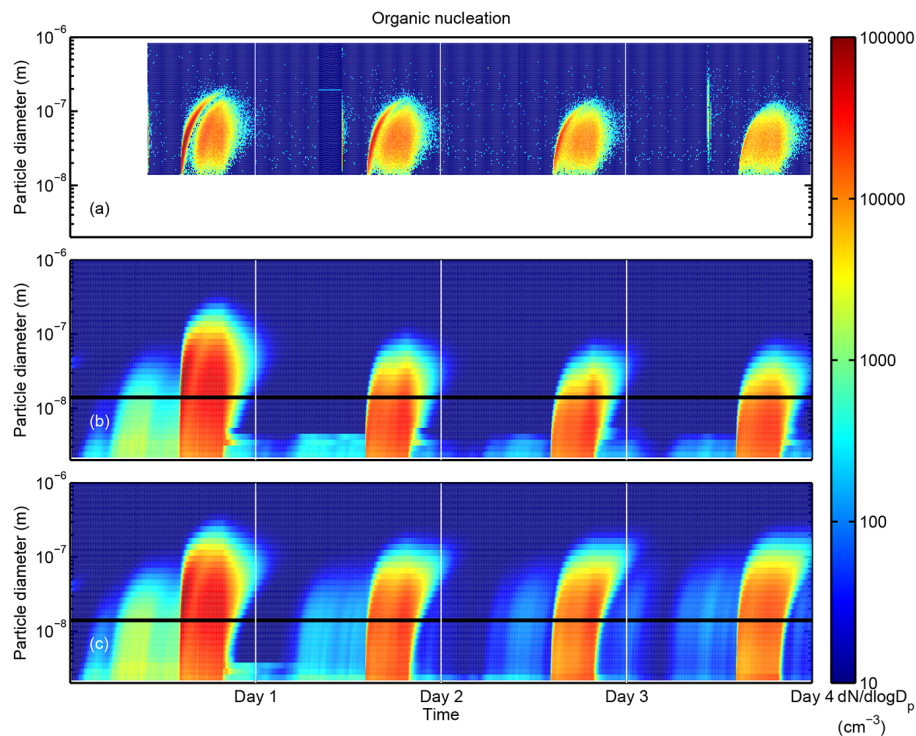


**Figure 11.** Contour plots of aerosol particle number size distributions as function of time from the SMPS measurements **(a)**, and contour plots of aerosol particle number size distributions as function of time from the MALTE-BOX model predicted using organic nucleation without **(b)** and with **(c)** SVOC gas-wall-partitioning. The black lines indicate the smallest particle size measured by SMPS in all sub-figures.

Title Page

Abstract

Introduction

Conclusions

References

Tables

Figures

◀

▶

◀

▶

Back

Close

Full Screen / Esc

Printer-friendly Version

Interactive Discussion

## Modelling the contribution of biogenic VOCs to new particle formation

L. Liao et al.

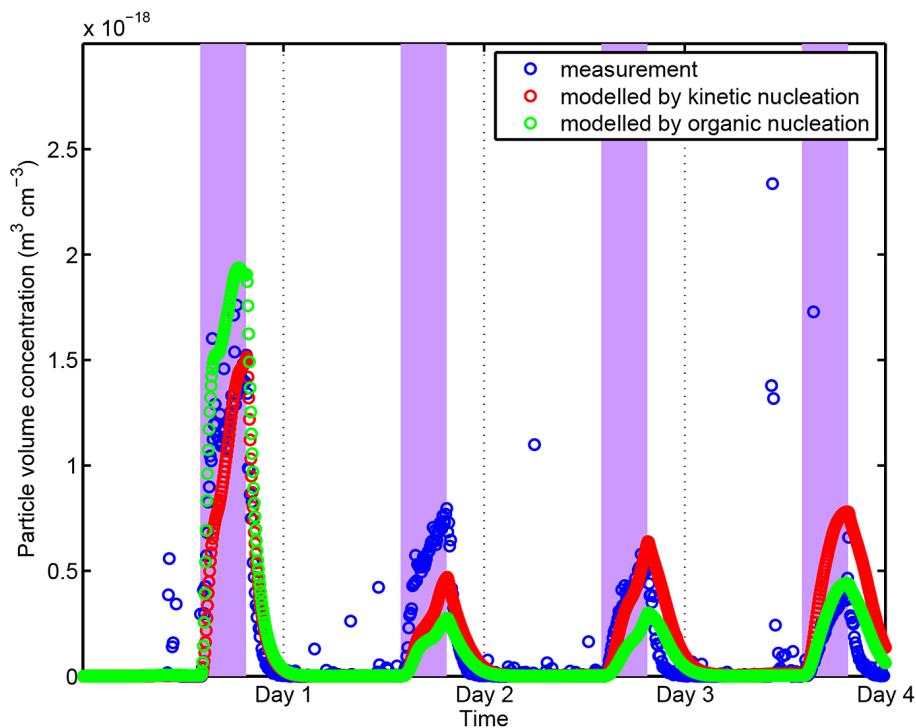


**Figure 12.** Time series of the total aerosol volumes modelled and measured. The blue markers indicate the total aerosol volumes calculated from the SMPS measurements. The red markers represent the particle volumes predicted by the model using kinetic H<sub>2</sub>SO<sub>4</sub> nucleation, and the green markers are particle volumes predicted by the model using organic nucleation. The purple bars indicate UV-on periods during the measurements.

[Title Page](#)[Abstract](#)[Introduction](#)[Conclusions](#)[References](#)[Tables](#)[Figures](#)[◀](#)[▶](#)[◀](#)[▶](#)[Back](#)[Close](#)[Full Screen / Esc](#)[Printer-friendly Version](#)[Interactive Discussion](#)

## Modelling the contribution of biogenic VOCs to new particle formation

L. Liao et al.

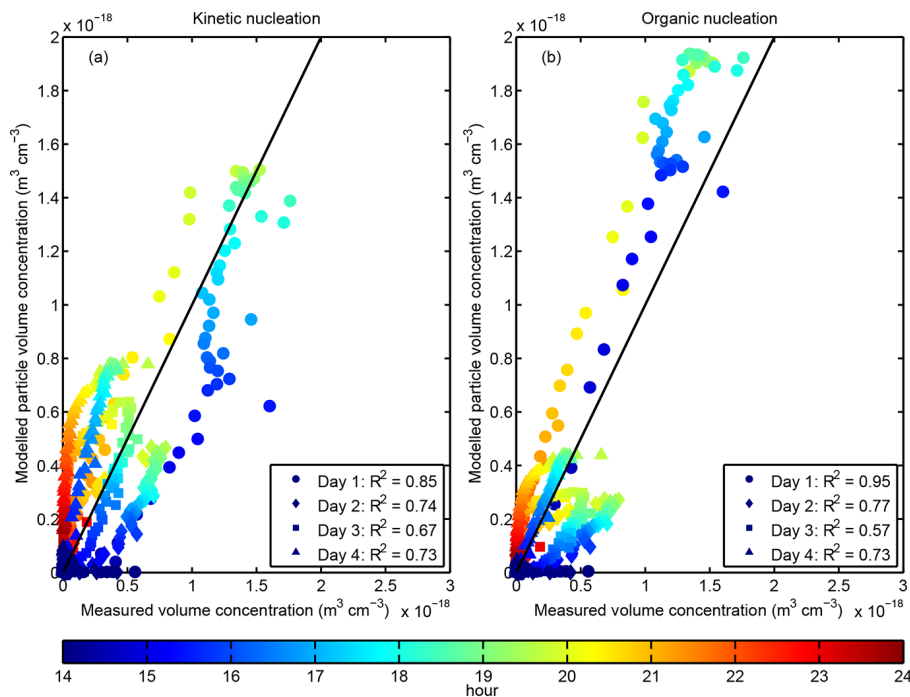


**Figure 13.** Total particle volume concentrations modelled **(a)** using kinetic  $\text{H}_2\text{SO}_4$  nucleation and **(b)** using organic nucleation vs. total particle volume concentrations calculated from SMPS measurements. The black lines indicate the 1 : 1 ratio in both figures. The coefficients of determination ( $R^2$ ) are listed in the legends. The color bar indicates hours of the day.

## Modelling the contribution of biogenic VOCs to new particle formation

L. Liao et al.

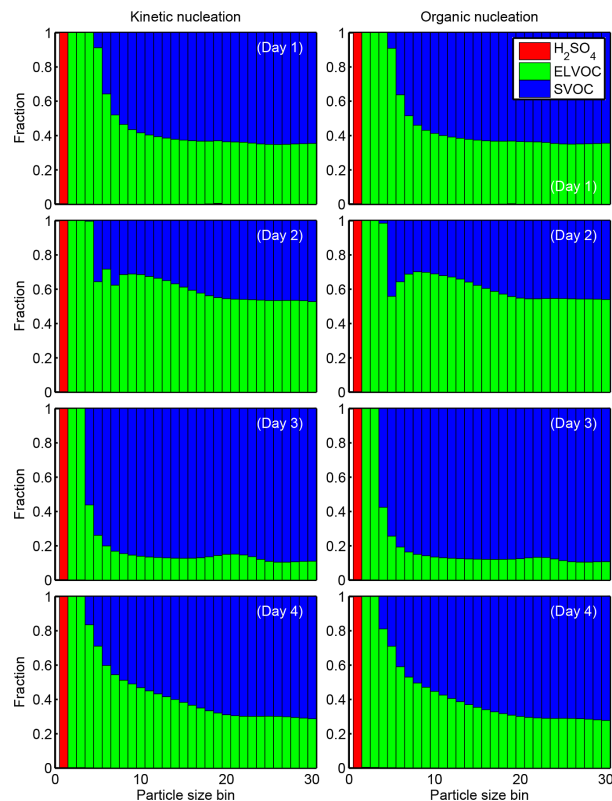


**Figure 14.** Volume fraction of the particle compositions both from the kinetic  $\text{H}_2\text{SO}_4$  nucleation and organic nucleation during UV-on periods from Day-1 to Day-4. The red bars indicate the total volume fraction of  $\text{H}_2\text{SO}_4$ , green bars illustrate the volume fraction of ELVOCs, and blue bars depict the volume fraction of SVOCs.

[Title Page](#)[Abstract](#)[Introduction](#)[Conclusions](#)[References](#)[Tables](#)[Figures](#)[◀](#)[▶](#)[◀](#)[▶](#)[Back](#)[Close](#)[Full Screen / Esc](#)[Printer-friendly Version](#)[Interactive Discussion](#)